Journal of Molecular Liquids xxx (xxxx) xxx

Contents lists available at ScienceDirect

Journal of Molecular Liquids

journal homepage: www.elsevier.com/locate/molliq

High temperature polymorphic conversion of carbamazepine in supercritical CO_2: A way to obtain pure polymorph I

Roman D. Oparin [a,*], Yevhenii A. Vaksler [b,c], Michael A. Krestyaninov [a], Abdenacer Idrissi [b], Michael G. Kiselev [a]

[a] G.A. Krestov Institute of Solution Chemistry of the Russian Academy of Sciences (RAS), Akademicheskaya str. 1, Ivanovo 153045, Russia
[b] Laboratoire de Spectroscopie pour les Interactions, la Réactivité et L'environnement (UMR CNRS A8516), Université Lille, 59655 Villeneuve d'Ascq Cedex, France
[c] V.N. Karazin Kharkiv National University, 4 Svobody Sq., Kharkiv 61022, Ukraine

ARTICLE INFO

Article history:
Received 5 September 2020
Received in revised form 16 October 2020
Accepted 18 October 2020
Available online xxxx

Keywords:
Carbamazepine
Supercritical carbon dioxide
Polymorphism
Conformational equilibrium

ABSTRACT

In this work, we studied the high-temperature polymorphic conversion of carbamazepine (CBZ) in a high-density supercritical CO_2 ($scCO_2$) medium in the temperature range of 110–200°C. In order to understand the mechanism of transformation we performed a detailed IR analysis of the supercritical fluid (SCF) phase being in permanent contact with an excess of CBZ. We studied the conformational equilibrium of CBZ molecules in $scCO_2$ phase under isochoric heating conditions. Three temperature ranges, where different types of CBZ–$scCO_2$ equilibria are realized, were considered: i. «CBZ solid – SCF solution»; ii. phase transition region related to the melting of CBZ in high-density $scCO_2$; iii. «CBZ melt – SCF solution». An analysis of the IR spectroscopy data on CBZ dissolved in the $scCO_2$ phase obtained for the third temperature range shows that when «CBZ melt – SCF solution» equilibrium exists, the $scCO_2$ phase contains only one CBZ conformer. Relying on this finding, we hypothesized that it is possible to obtain pure CBZ polymorph I by the crystallization from CBZ solution in $scCO_2$. This statement has been proven by the micro-Raman analysis of the crystalline substance being obtained from such fluid solution.

1. Introduction

Studying of drug compounds polymorphism is of particular importance even at the stage of pharmaceutical synthesis before the final product enters the pharmaceutical market [1,2]. It is due to the fact that various physical, chemical and biological properties of the active pharmaceutical ingredient (API), such as biological activity, stability, solubility and bioavailability are closely related to the drug compound polymorphism [3–6].

The increased interest in using supercritical fluid (SCF) processes for drug synthesis arises from several important advantages of the SCF technologies. SCF systems, in particular, the ones based on supercritical carbon dioxide ($scCO_2$), are used as a promising non-toxic eco-friendly alternative to organic solvents utilized in classical crystallization methods [7–14]. Indeed, a target product purification from organic solvents requires numerous time-consuming or expensive steps, and even after purification they can contain residual of solvent with low concentration (about 10^{-5} of molar fractions) but still dangerous for human, because of possible cumulative effect at longtime therapy. For example, our recent spectral analysis of paracetamol with ≥99% of purity dissolved in $scCO_2$ showed the presence of amide solvent traces. On the contrary, CO_2 is quite easily removed from a target compound at the end of the synthesis procedure, transferring from supercritical state to gaseous one (at cooling down and depressurizing). It allows excluding the purification stage from technological process, making $scCO_2$ to be a suitable medium for the producing the «pure» drug forms.

Along with polymorphism, one of important characteristic of organic substances, in particular, drugs, is conformational state of their molecules in solutions, which is closely related to polymorphism of drug crystalline forms being obtained from those solutions. We have recently performed a series of studies of the conformational equilibria and polymorphism of drug compounds in a $scCO_2$ medium [15–20] and in a number of organic solvents [21–23]. We demonstrated that by characterizing the processes occurring at the drug-$scCO_2$ interface, in particular by quantifying the distribution of the conformers of the drug that are dissolved in the CO_2 phase at different thermodynamic state parameters, the polymorphism of the API crystalline phase can be controlled.

One of the compounds we studied was carbamazepine (CBZ). This compound can crystallize in 5 different polymorphs [24–29]. However, they differ only in the orientation of the molecules in the crystal structures and have rather low conformational flexibility. Polymorph III of

Abbreviations: CBZ, carbamazepine; HPHT, high pressure high temperature; ICA, isocyanic acid; IMST, iminostilbene (dibenzazepine); IMST–H^+, iminostilbene protonated form; QCC, quantum chemical calculations; RESS, rapid expansion of supercritical solution; $scCO_2$, supercritical carbon dioxide; SCF, supercritical fluid.

* Corresponding author.
E-mail address: r.d.oparin@yandex.ru (R.D. Oparin).

https://doi.org/10.1016/j.molliq.2020.114630
0167-7322/

CBZ is the only one used in pharmaceutics nowadays as the most stable at room temperature. However, polymorph I that is less stable at room temperature [30], could be more interesting pharmacologically, e.g. in composites with polymers, where it can be stabilized by polymer matrix.

In our work [18], we showed that metastable polymorphic form I can be obtained from polymorphic form III by recrystallization through the solution in $scCO_2$ at a temperature of 110°C. This process can be formally separated into two principal stages. At the first stage, CBZ form III was dissolved in $scCO_2$. This led to the conformational equilibrium of the CBZ molecules in the $scCO_2$ phase due to the thermodynamic factor. The second stage consisted of crystallization of the CBZ polymorphic form I that is the most stable in the given conditions from the SCF solution. We also showed that the temperature and density of the CO_2 phase significantly affect the solubility of CBZ in $scCO_2$, and the temperature has an influence on the dissolution kinetics. Thus, the yield of polymorph I directly depends on the fluid phase density and temperature. Despite the fact that the use of the considered approach makes it possible to produce polymorph I, it is always possible to obtain the initial form as a side product. This situation will remain so while there is conformational equilibrium in the SCF solution. It is possible to completely shift this equilibrium towards the conformer being present in polymorph I by increasing the temperature. For example, in our previous study [17] of the conformational equilibria of mefenamic acid (MA) in a $scCO_2$ medium, we showed that there is only one conformer in the solution phase at a temperature above the MA melting point. This conformer determines the formation of MA metastable form II through crystallization from its SCF solution. In the present study, we will also attempt to create the same conditions that will allow us to obtain a similar result for CBZ.

Assuming that the increase in the temperature of the CBZ–$scCO_2$ binary mixture will shift the equilibrium in the $scCO_2$ phase towards the conformer corresponding to polymorph I, we can expect that CBZ crystallization from the $scCO_2$ phase (for example, via Rapid Expansion of Supercritical Solution RESS) will produce «pure» polymorph I. Moreover, one can expect that at high temperatures the time required for reaching the CBZ equilibrium concentration in $scCO_2$ will be significantly less compared with the low-temperature process (at 110°C), as it was described in work [18]. As a consequence, the total process time can be also significantly reduced.

Thus, the main aim of this study was to evaluate the possibility of preparing CBZ polymorph I from CBZ saturated solution in $scCO_2$ at the temperatures above the CBZ melting point. Consequently, in order to study the high-temperature conformational equilibria of CBZ in $scCO_2$, we expanded the temperature range studied in work [18] to 200°C.

To achieve this aim we set out to do the following tasks:

- To study in details the conformational equilibria of the CBZ molecules in the $scCO_2$ medium in a two-phase CBZ–$scCO_2$ mixture under isochoric heating (at a constant CO_2 density equal to 1.3 of its critical value) in the temperature range from 110 to 200°C, including the region of the CBZ phase transition associated with its melting.
- To analyze the polymorphic composition of the solid CBZ phase obtained by CBZ crystallization from the SCF solution, using micro-Raman spectroscopy.

2. Materials

The CO_2 gas (99.99% purity) was purchased from "The Linde Group". The powder of the CBZ form III (5H-Dibenz[*b*,*f*]azepine-5-carboxamide) was purchased from "Sigma-Aldrich" (CAS Number 298-46-4). According to the DSC results presented in Ref. [30], the first endothermic peak appears at 174.8°C and immediately followed by an exothermic peak, the second endothermic peak appears at 193.2°C (see Fig. 1). The results of the thermomicroscopy also presented in this work showed that form III melts and subsequently crystallizes to form I from 162 to 175°C (*endo*-exo melting-recrystallization). In turn form I melts between 189 and 193°C. Thus, the first endothermic peak on the DSC curve corresponds to the melting of form III, whereas the exothermic peak is attributed to the crystallization of form I, which melting gives the second endothermic peak on DSC curve. Though, there is a certain discrepancy between hot-stage and DSC measurements, which might have arisen from various heating rates and/or other experimental parameters being used in this work, nevertheless these data give us a useful initial information on high-temperature conversion of CBZ from form III to form I under atmospheric pressure.

3. Experimental part

3.1. 3.1. Visual analysis of the structural changes in the CBZ sample

The thermal changes in the CBZ surface permanently contacting with CBZ saturated solution in $scCO_2$ were visually observed with the help of the system specially designed by us. It is based on a digital long-focus optical microscope. This microscope is united with a universal High-Pressure-High-Temperature (HPHT) optical cell via a precise positioning system. Moreover, the microscope is also equipped with coaxial brightening that allows making a bright image of a target placed deep inside the optical cell. The HPHT cell is equipped with an optically transparent sapphire window enabling to take a photo of the CBZ surface inside the cell. Its thickness of 9 mm in combination with a small diameter (the external diameter is 12 mm and the effective working diameter is 8 mm) allows to work at pressures of up to 1 kbar inside the cell. A detailed description of the optical cell and window sealing system is presented in our previous publication [17]. To control the temperature and pressure of the reaction medium inside the cell, we used the experimental setup that was successfully applied in a number of our works [15,17,19]. The photos of the CBZ surface permanently contacting with CBZ saturated solution in $scCO_2$ were made with an optical resolution of 2 megapixels. The images were obtained for a number of temperatures along the chosen isochore. These photos are presented in Fig. 2.

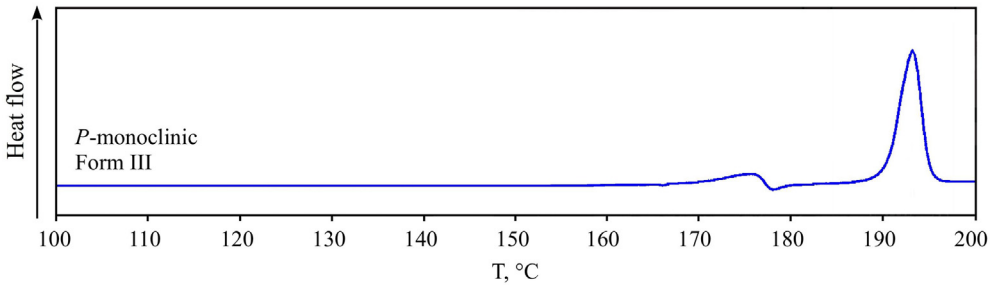

Fig. 1. DSC profile of CBZ polymorph III measured at atmospheric pressure [30].

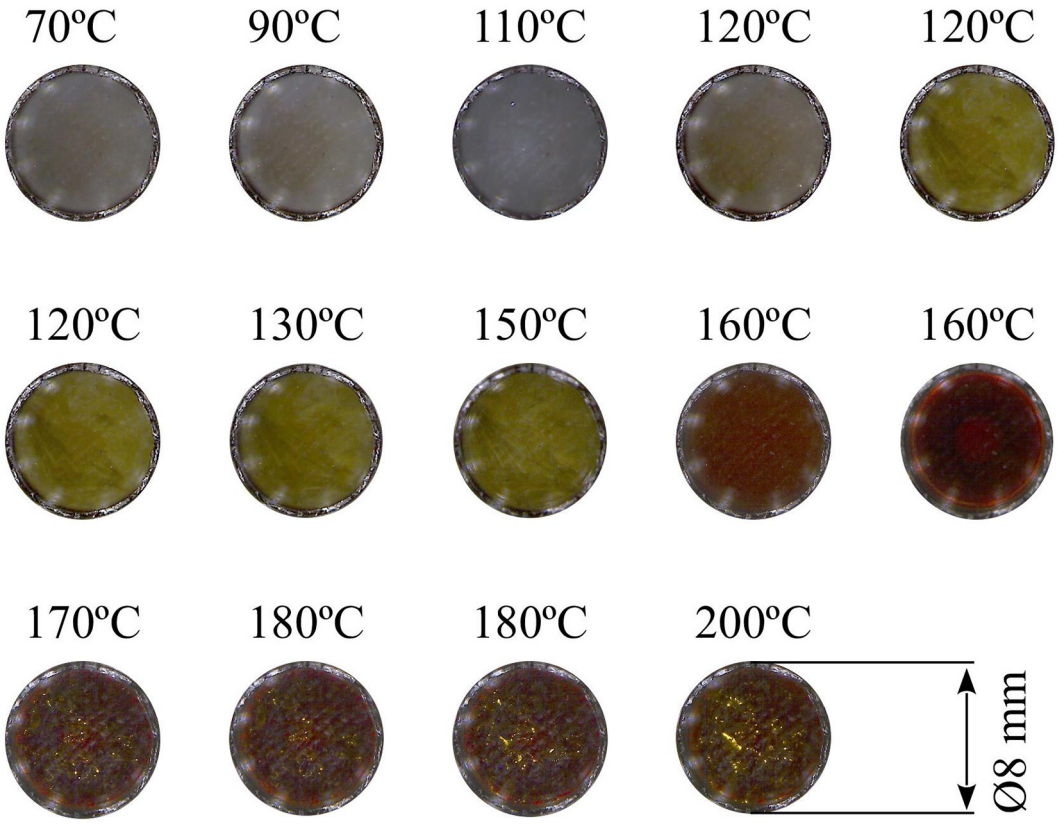

Fig. 2. Photos of the thermal change's evolution in the CBZ surface permanently contacting with CBZ saturated solution in $scCO_2$ when heated along the chosen isochore. The photos correspond to the equilibrium state. For the key temperatures of 120, 160, 180°C we presented the series of photos with a time step of 12 h to demonstrate the dynamics of the changes.

By analyzing the photos presented in Fig. 2, three temperature ranges were identified. In the temperature range of 70–110°C, no changes are observed at the CBZ surface. However, at the temperature of 120°C, the surface takes on a yellow tint, the intensity of which considerably increases while this temperature is maintained. In the temperature range of 120–150°C, the surface color remains unchanged. The yellow color of the CBZ surface is the evidence of CBZ thermal degradation, with solid iminostilbene (IMST) and volatile isocyanic acid (ICA) formed as a result of the decomposition reaction (deamidation process) (see Fig. 3). This is one of the most probable pathways of CBZ degradation described in the literature (see, e.g., Refs. [31–34]).

The heating to 160°C considerably changes the color of the CBZ surface, while maintaining this temperature for another 12 h leads to the total melting of the CBZ crystalline phase. It is also important to note that this temperature is lower than the melting temperature of polymorph III as was shown above. We mentioned such decrease in the melting temperature of pharmaceuticals in our previous works [16,17]. This fact is in good agreement with works [35–37], where the authors noted the reduction in the melting temperatures of organic solids in a high-pressure CO_2 medium. They attributed this to the increase in the CO_2 dissolution capacity with an increase in its density. Further heating from 160°C to 200°C results in the sedimentation of small yellow crystals of IMST. Along with this in the temperature range of 160–200°C melt CBZ phase remains stable and its crystallization does not occur.

3.2. In situ IR spectroscopy of CO_2-rich phase of the CBZ–$scCO_2$ binary system

To study the conformational equilibrium of CBZ molecules in the $scCO_2$ phase permanently contacting with an excess of solid CBZ under isochoric heating, we used the same experimental setup [15,17,19] and the HPHT IR optical cell described in detail in Ref. [17]. To prepare the initial binary mixture of CBZ and $scCO_2$ we followed

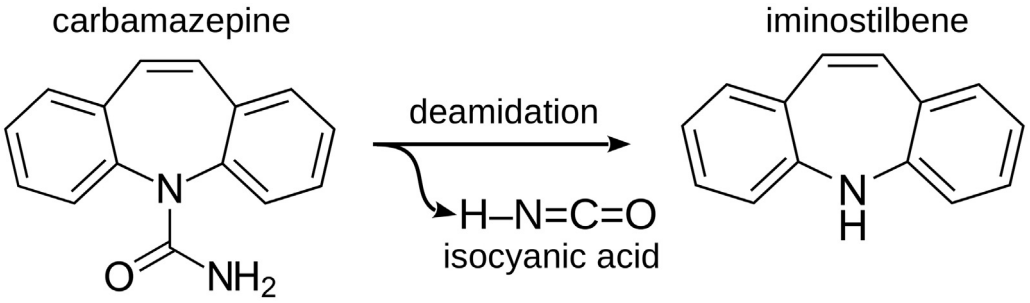

Fig. 3. CBZ degradation pathway (deamidation) leading to the formation of IMST and ICA.

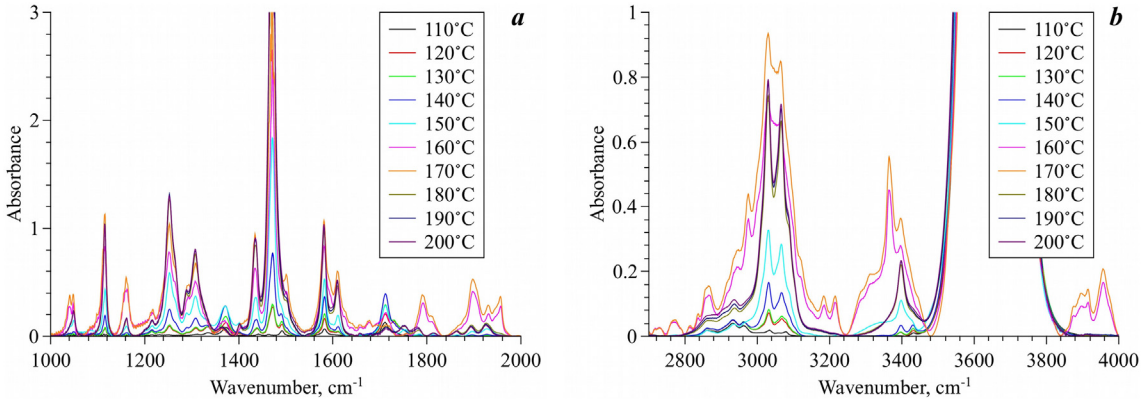

Fig. 4. IR spectra of CBZ dissolved in the $scCO_2$ phase permanently contacting with an excess of CBZ in isochoric heating conditions in the temperature range of 110–200°C (ΔT=10°C) along the chosen isochore for two spectral ranges: (***a***) 1000–2000 cm^{-1} and (***b***) 2700–4000 cm^{-1}.

the procedure described in our previous works (see Refs. [18, 19]). In order to prepare the CBZ–$scCO_2$ mixture with a permanent excess of CBZ, we measured the CBZ solubility in $scCO_2$ [38]. The IR spectra of the $scCO_2$-rich phase (SCF solution phase) of two-phases systems of "CBZ solid – SCF solution" or "CBZ melt – SCF solution" depending on parameters of state were measured. Bruker Vertex 80v FTIR spectrometer equipped with a vacuum sample chamber was used. Vacuum sample chamber excludes the influence of the atmospheric water vapor and carbon dioxide on the measured spectra.

The spectra with a high signal-to-noise ratio were recorded in the wavenumber range of 1000–4000 cm^{-1} with a resolution of 1 cm^{-1} in the temperature range of 110–200°C with a step of 10°C along the chosen isochore. For each temperature, we recorded the IR spectrum every 30 min until the spectra remained unchanged in the last 3–4 measurements. Thus, the temperature/time program ran for the experiments was as follows: 110°C – 12 h, 120°C – 30 h, 130°C – 6 h, 140°C – 30 h, 150°C – 30 h, 160°C – 15 h, 170°C – 12 h, 180°C – 5 h, 190°C – 5 h, 200°C – 5 h. As in our previous works, in this study, we used the same optical path length of the sample (0.1 cm) that was optimized in order to exclude the oversaturation of the spectral bands in the spectral domains of interest within the whole investigated temperature range. The final spectra of CBZ dissolved in $scCO_2$ were obtained by direct subtraction of the neat CO_2 spectra from the CBZ–CO_2 binary mixture spectra measured in the same thermodynamic conditions. The obtained spectra are presented in Fig. 4.

A preliminary analysis of the spectra shown in Fig. 4 in combination with the data presented in chapter 2.1 allowed us to identify 3 key temperature ranges: 110–150°C, 150–170°C, and 170–200°C, where the character of the spectral changes is different. Moreover, we determined the spectral domains - 1350–1850 cm^{-1} and 3250–3550 cm^{-1}, which will be used as analytical ones in the conformational analysis. In the series of our studies directed towards conformational analysis of drug molecules in CO_2 phase we used a combination of the results of IR spectra analysis and quantum chemical calculations (QCC) (see, e.g., Refs. [15–19]).

3.3. Quantum chemical calculations

First of all, in this study we used the results of QCC that were performed in our previous work [18], where we determined two most stable conformers of CBZ – Conf. 1 and Conf. 2. The differences between these two conformers can be determined by the dihedral angles of τ1, τ2 and τ3 (see Fig. 5). Their values are presented in Table 1. It was that the first conformer has lower energy, and the energy difference between these two conformers is 1.49 $kJ \cdot mol^{-1}$. For them we calculated the IR spectra and identified the key analytical IR spectral bands,

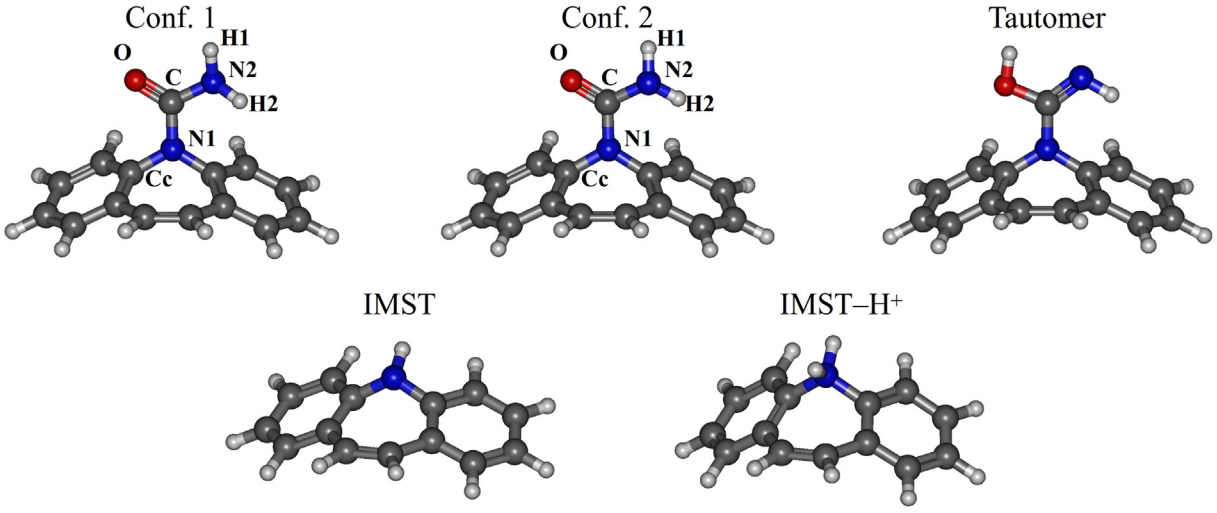

Fig. 5. The optimized molecular structures of two CBZ conformers (Conf. 1 and Conf. 2) with different orientation of the hydrogen atoms of the amide group, CBZ tautomeric form, iminostilbene (IMST), and its protonated form (IMST–H^+). The differences between these two conformers can be determined by the values of the dihedral angles τ1 (N1-C-N2-H1), τ2 (N1-C-N2-H2) and τ3 (Cc-N1-C-O).

Table 1
Values of dihedral angles τ1, τ2 and τ3 (see Fig. 3) for two CBZ conformers as obtained by QCC.

	τ1	τ2	τ3
Conf. I	−165.8°	−24.0°	−7.0°
Conf. II	166.7°	15.7°	−10.4°

whose behavior is sensitive to the conformational transitions of the CBZ molecule. Taking into account the CBZ thermal degradation, leading to the formation of IMST, and applying the same calculation approach, as described in Ref. [18], in the present work we additionally optimized the geometry and calculated the vibration frequencies for IMST and for its protonated form (IMST–H^+). Moreover, relying on the possibility of the CBZ tautomerization that should occur via proton transfer in the carboxamide group from the amide nitrogen to carbonyl oxygen (see, e.g., Ref. [33]), we also performed calculations of the molecular structure and vibration frequencies for the most probable CBZ tautomer (see Fig. 5). All the calculations were performed in the GAUSSIAN 09 suite of programs [39], using the APFD functional [40] (which includes the Petersson-Frisch dispersion correction model) with the 6–311++g (2d,p) basis set. For all these molecular structures we also calculated the IR spectra and compared them to those obtained for Conf. 1 and Conf. 2 (see Fig. 6 and Table 2.).

4. Spectral analysis and discussion

4.1. Temperature range of 110–150°C

Fig. 7 illustrates the thermal evolution of the IR spectra of CBZ dissolved in the $scCO_2$ phase in the temperature range of 110–150°C. Based on the IR spectra obtained by QCC we determined the key analytical spectral bands. The assignments of these spectral bands (see Table 3) were performed based on the data presented in Table 2.

An analysis of the thermal evolution of the spectra presented in Fig. 7 allowed us to identify the appearance of the CBZ tautomeric form in the $scCO_2$ phase beginning from 120°C. Further heating up to 140°C reduces the spectral contributions related to CBZ Conf. 1, whereas the intensity of the spectral contributions related to the CBZ tautomeric form considerably increases. Moreover, at this stage two points related to the thermal degradation of CBZ deserve to be also clarified. The analysis of the IR spectra didn't allow us to identify the spectral signatures of IMST, despite the appearance of yellow tint (associated with IMST) at the surface of the CBZ solid form beginning from 120°C as shown in Fig. 2. It means that IMST is not present in the $scCO_2$ phase.

Concerning the ICA component, we will discuss in more details the problems we were faced to prove its presence in the $scCO_2$ phase. According to the QCC, the most intensive spectral bands related to the vibrations of gaseous ICA (boiling point T_b = 23.5°C [41]) are either situated beyond the transmission band of silicon (~1000–8300 cm^{-1}), the material the optical windows of the IR cell are made from, or totally overlap with the spectral bands of the other component of the system. The first case is related to the δ(C=N–H) spectral band of ICA having a maximum at 812.46 cm^{-1} (see Table 2). In the second case, the spectral band of ν_{as}(O=C=N) (maximum at 2344.96 cm^{-1}) for the ICA molecule is completely overlapped by the oversaturated spectral band of ν_3 (CO_2) lying in the wavenumber range of 2100–2600 cm^{-1}. Another spectral band of ν(N—H) (with the maximum at 3703.26 cm^{-1}) for the ICA molecule is completely overlapped by the intensive spectral band of the CO_2 combinational diad ($2\nu_2\nu_3+\nu_1\nu_3$) lying in the wavenumber range of 3500–3850 cm^{-1} (see Fig. 4).

Nevertheless, according to Refs. [42, 43], a tautomeric equilibrium between ICA and cyanic acid (CA) is possible (H—N=C=O ↔ N≡C—O—H), where ICA is more stable, as shown by the QCC [44]. Thus, we can expect the appearance of CA bands on the IR spectrum along with ICA spectral bands. Indeed, starting from 120°C two spectral bands centered at 1088 cm^{-1} and 1231 cm^{-1} appear on the IR spectrum. According to our QCC and database [45], these two bands can be assigned to δ(C—O—H) and ν(C—O) of CA. Also, QCC give two more spectral bands related to CA, namely ν(N≡C) with a maximum at 2389.32 cm^{-1} and ν(O—H) with a maximum at 3810.36 cm^{-1}. However, as it was shown above, these two bands cannot be observed in the spectrum due to their overlapping with ν_3 spectral mode of CO_2 and the combinational diad ($2\nu_2\nu_3+\nu_1\nu_3$) of CO_2, respectively.

Starting from 150°C, the intensity of the spectral contributions that are related to CBZ Conf. 1 reaches the lower identification threshold. Along with this, the total spectral intensity increases. It is accompanied by the appearance of a wide shoulder on the low-frequency slope of the ν(N—H) spectral band of the CBZ tautomeric form. Such a drastic change in the spectral behavior is associated with the criticality phenomena, more specifically, with the appearance of the critical opalescence in the CO_2 phase. Similar behavior was explained in detail in our previous work [17].

4.2. Temperature range of 150–170°C

Subsequent increase in the temperature from 150 to 170°C results in a strong increase in the total spectral intensity of CBZ dissolved in the $scCO_2$ phase (see Fig. 8). This behavior is related to the phase transition region, namely, the melting of crystalline CBZ contacting the CO_2 phase. It is also proved by the results of visual control presented in Fig. 2 that show CBZ melting at 160°C.

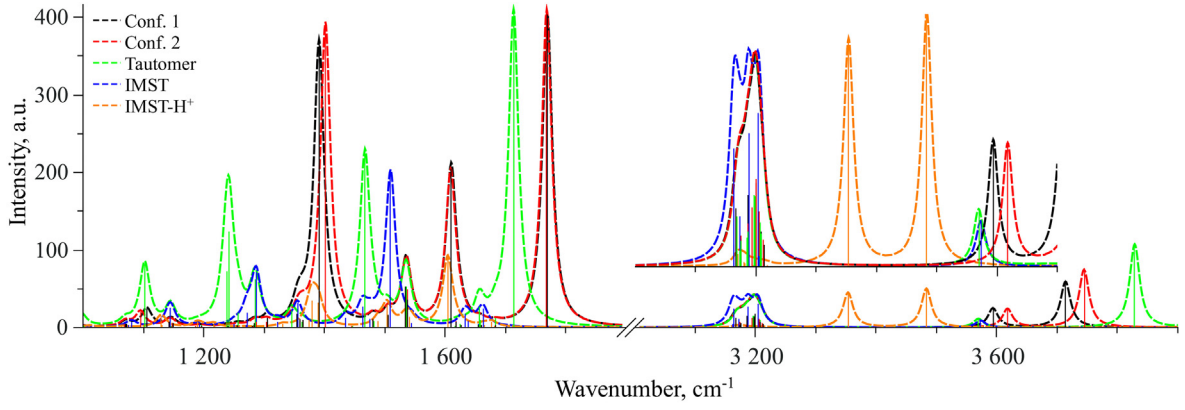

Fig. 6. The set of vibrational bands calculated via QCC (straight vertical lines) for two CBZ conformers (Conf. 1 and Conf. 2), CBZ tautomeric form, IMST, and IMST–H^+. The insertion shows the scaled spectral domain in the range of 3000–3700 cm^{-1}. The dashed lines, which are the set of Lorentzian bands with arbitrary dispersion, are presented for convenience.

Table 2
Peak maximum positions (frequency, cm^{-1}), intensities and assignments of the analytical spectral bands for molecular structures (see Fig. 5) as obtained by QCC.

Conf. 1	Conf. 2	Tautomer	IMST	IMST–H^+
1390.96 cm^{-1} 366.68 δ(C–N–H1)	1401.59 cm^{-1} 390.26 δ(C–N–H1)			
		1467.06 cm^{-1} 223.11 δ(C–O–H)+δ(C=N–H)		
			1509.42 cm^{-1} 200.23 aromatic + ρ(N—H)	
				1604.28 cm^{-1} 91.64 δ(H–N–H^+)
		1713.21 cm^{-1} 407.54 ν(C=N)		
1769.17 cm^{-1} 402.99 ν(C=O)	1768.10 cm^{-1} 408.77 ν(C=O)			
			3164.06 cm^{-1} 23.33 ν (C—H) 3187.88 cm^{-1} 26.29 ν (C—H)	
		3569.67 cm^{-1} 11.17 ν(N—H)	3573.27 cm^{-1} 8.99 ν(N—H)	
3593.76 cm^{-1} 24.68 ν_s(H—N—H) 3713.97 cm^{-1} 59.15 ν_{as}(H–N–H)	3617.83 cm^{-1} 24.00 ν_s(H–N–H) 3744.68 cm^{-1} 74.56 ν_{as}(H–N–H)			3353.73 cm^{-1} 44.92 ν_s(H–N–H^+) 3483.57 cm^{-1} 50.05 ν_{as}(H–N–H^+)
		3828.53 cm^{-1} 107.40 ν(O—H)		

Here we denoted the different types of vibration as follows: δ is a scissoring vibration; ν is a stretching vibration; ν_s is a symmetric stretching vibration; ν_{as} is an antisymmetric stretching vibration; δ(C–O–H)+δ(C=N–H) is an antiphase scissoring vibration; aromatic+ρ(N—H) is a complex vibration.

Moreover, one of the interesting peculiarities characterizing the spectra of the CBZ–$scCO_2$ binary mixture in this temperature range is the appearance of new spectral contributions related to the CBZ thermal degradation products (see Fig. 8). These new contributions were identified in both analytical spectral domains and were attributed to the vibrations of the functional groups of IMST and IMST–H^+ (see Table 4). It is also necessary to note that the complex band related to the ν(C—H) vibrations has an obvious difference for CBZ and IMST in the spectral domain of 2800–3225 cm^{-1}. Namely, when IMST appears in the system, two additional intensive spectral contributions arise at the low-frequency side of the CBZ ν(C—H) band (see Fig. 6).

4.3. Temperature range of 170–200°C

The analysis of the spectral changes in the temperature range of 170–180°C (see Fig. 9) showed a considerable decrease in the total spectral intensity. Along with this, the spectral bands, which are related to the vibrations of IMST and IMST–H^+ completely disappear. The wide

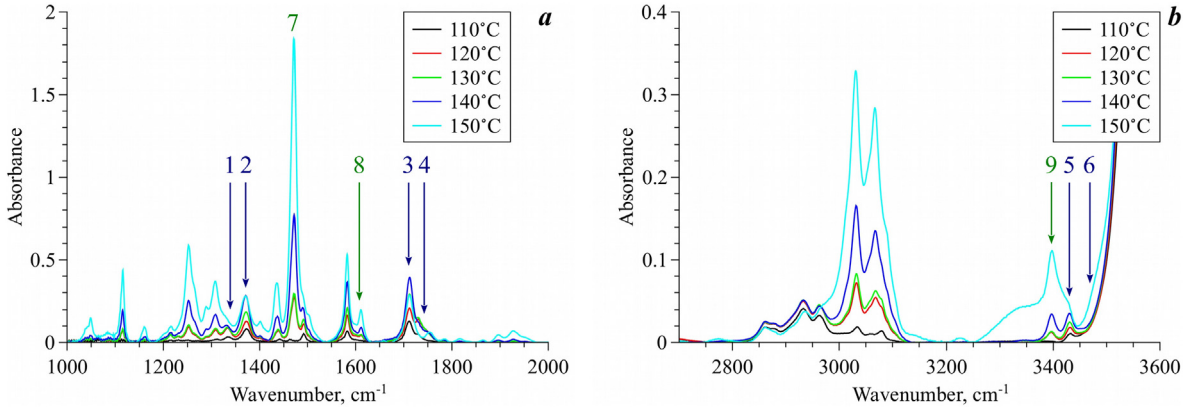

Fig. 7. IR spectra of CBZ dissolved in the $scCO_2$ phase permanently contacting with an excess of CBZ in isochoric heating conditions in the temperature range of 110–150°C (Δ*T*=10°C) along the chosen isochore for two spectral ranges: (***a***) 1000–2000 cm^{-1} and (***b***) 2700–3600 cm^{-1}. The arrows with numbers show the analytical spectral bands determined by QCC.

Table 3
The assignment of the spectral bands in two analytical spectral domains (1350–1850 cm^{-1} and 3250–3550 cm^{-1}) of the experimental spectra based on the QCC results presented in Table 2.

1350–1850 cm^{-1}	3250–3550 cm^{-1}
1– δ(C–N–H1) of Conf. 1	**5**– ν_s(H–N–H) of Conf. 1
2– δ(C–N–H1) of Conf. 2	**6**– ν_s(H–N–H) of Conf. 2
3– ν(C=O) of Conf. 2	**9**– ν(N—H) of Tautomer
4– ν(C=O) of Conf. 1	
7– δ(C–O–H)+δ(C=N–H) of Tautomer	
8– ν(C=N) of Tautomer	

Table 4
The assignments of the experimental spectral bands related to the vibrations of the functional groups of IMST and IMST–H^+ in two analytical spectral domains (1350–1850 cm^{-1} and 3250–3550 cm^{-1}) based on the QCC results are presented in Table 2. The additional spectral domain of 2800–3225 cm^{-1} shows a set of unique spectral contributions of ν(C—H) that exist only in the IMST spectrum (see Fig. 6 and Table 2).

1350–1850 cm^{-1}	2800–3225 cm^{-1}	3250–3550 cm^{-1}
10– aromatic system vibration +ρ(N—H) of IMST	**12**– ν(C—H) of IMST	**13**– ν_s(H–N–H^+) of IMST–H^+
11– δ(H–N–H^+) of IMST–H^+		**14**– ν_{as}(H–N–H^+) of IMST–H^+
		15– ν_s(N—H) of IMST

shoulder on the low-frequency slope of the ν(N—H) spectral band of the CBZ tautomeric form as well as the spectral contributions related to Conf. 2 also vanished. As a result, the CBZ tautomeric form prevailed in the $scCO_2$ phase.

Further heating from 180 to 200°C the spectral changes become monotonous that is generally typical of the thermal evolution of the equilibrium spectra. This behavior is the evidence of the CBZ concentration increase in the CO_2 phase, at that it is not accompanied by CBZ conformational transitions. Similar spectral behavior above the drug melting point (above the phase transition region) was also demonstrated in our work about the conformational equilibrium of MA in the CO_2 phase under isochoric heating (see Ref. [17]).

It is important to note that the disappearance of the spectral contributions related to IMST and IMST–H^+ correlates with sedimentation from the $scCO_2$ phase of the yellow IMST crystals, the appearance of which is observed on the optical window surface at the temperature 170°C and above (see Fig. 2). Therefore, as far as only CBZ in the tautomeric form is present in the $scCO_2$ phase in the temperature range of 180–200°C, it may be expected that the crystallization from such a SCF solution should lead to the formation of pure CBZ polymorph I.

Thus, analyzing the data obtained for two systems: where solid-fluid equilibrium (CBZ solid – SCF solution) and liquid-fluid equilibrium (CBZ melt – SCF solution) are realized, we can assume that from a pharmaceutical perspective, especially in terms of fundamental understanding of such systems, the crystallization of pure polymorph I is more preferable from $scCO_2$ phase being in contact with CBZ melt. Indeed, taking into account our recent findings [17] as well as results of this work, one can see that in the case of CBZ melt – SCF solution system, in $scCO_2$ phase there is only one CBZ conformer, and crystallization from such solution will lead to formation of polymorph I. On the contrary, when the CBZ solid – SCF solution interface exists, in $scCO_2$ phase there is conformational equilibrium that can shift towards certain conformer depending on parameters of state, and it will lead to change of polymorphic modification of drug solid being crystallized.

In order to prove this hypothesis, we analyzed the crystalline phase that was obtained by cooling the experimental cell (from 200°C to the ambient temperature) with subsequent depressurization and pumping out of the residual CO_2. The crystalline sample extracted from the cell was a mixture of two crystalline structures (see Fig. 10): relatively large rhombic crystals (up to 0.5 mm) and long needle crystals (0.1×1 mm). These crystalline samples were studied by the micro-Raman spectroscopy technique.

4.4. Micro-Raman spectroscopy analysis

The Raman spectra were measured with a LabRAM HR Evolution Raman spectrometer combined with a confocal microscope (with a 100× magnifying objective). The signal was collected in the back-scattering geometry. A He—Ne laser (λ = 632.81 nm) with the maximum energy of 15 mW at the sample was applied for excitation. The spectra were measured in the spectral range of 50–3600 cm^{-1} with a final resolution of about 0.3 cm^{-1} that was achieved with the use of a diffraction grating of 1800 grooves/mm. In this series of measurements, the acquisition times, number of accumulations and laser beam power were varied according to the orientation and thickness of the sample in order to avoid its burning-out and to improve the signal-to-noise ratio. Then, the obtained Raman spectra were compared to that of pure CBZ polymorph III, as well as to the spectra measured from the crystalline CBZ surface permanently contacting with CBZ saturated solution in $scCO_2$ at the temperatures of 40, 110, and 120°C (as presented in Ref. [18]) (see Fig. 11).

The spectral range (3300–3600 cm^{-1}), that is associated with the stretching N—H vibrations, is more convenient for analyzing CBZ polymorphic forms. Indeed, in this spectral domain the characteristic spectral bands are well resolved and do not overlap each other (see Fig. 11***b***). An analysis of these spectra allowed us to conclude that the large rhombic crystals are IMST (the characteristic spectral band of

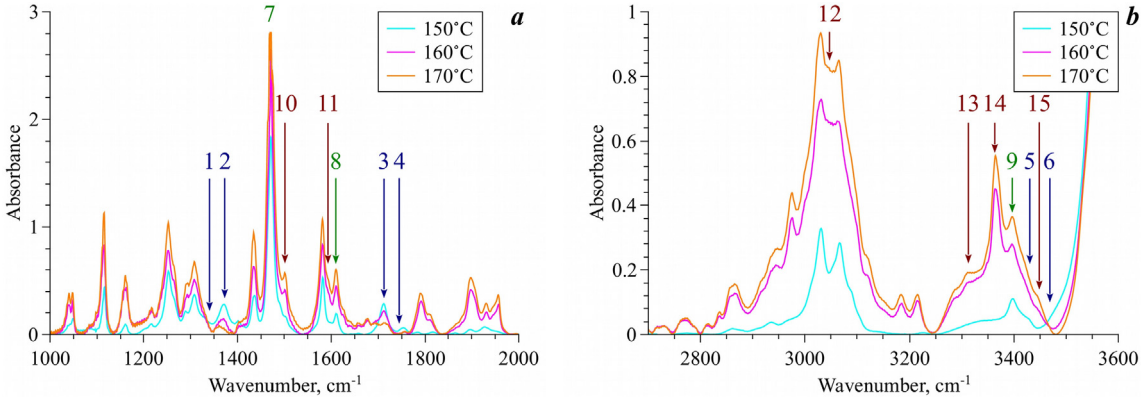

Fig. 8. IR spectra of CBZ dissolved in the $scCO_2$ phase permanently contacting with an excess of CBZ in isochoric heating conditions in the temperature range of 150–170°C (ΔT=10°C) along the chosen isochore for two spectral ranges: (***a***) 1000–2000 cm^{-1} and (***b***) 2700–3600 cm^{-1}. The arrows with numbers show the analytical spectral bands determined by the QCC. The assignments of these spectral bands are presented in Table 4.

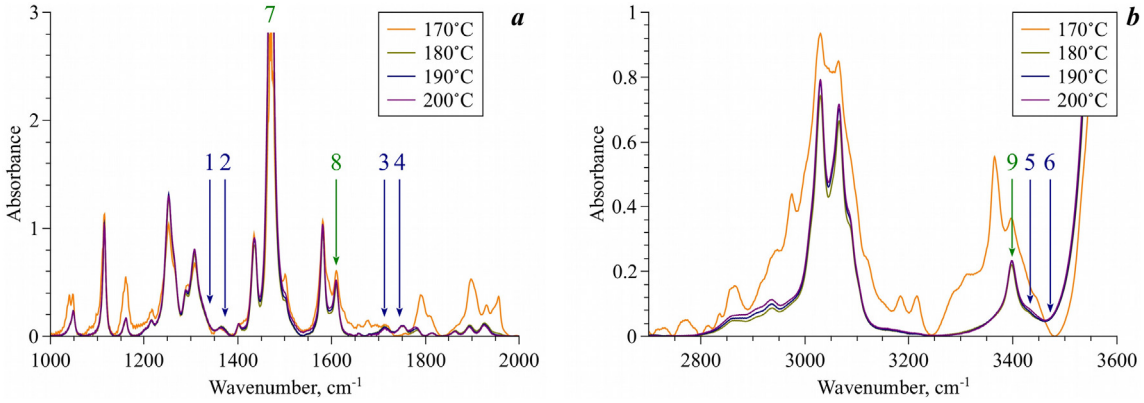

Fig. 9. IR spectra of CBZ dissolved in the $scCO_2$ phase permanently contacting with an excess of CBZ in isochoric heating conditions in the temperature range of 170–200°C (ΔT=10°C) along the chosen isochore for two spectral ranges: (***a***) 1000–2000 cm^{-1} and (***b***) 2700–3600 cm^{-1}. The arrows with numbers show the analytical spectral bands determined by QCC.

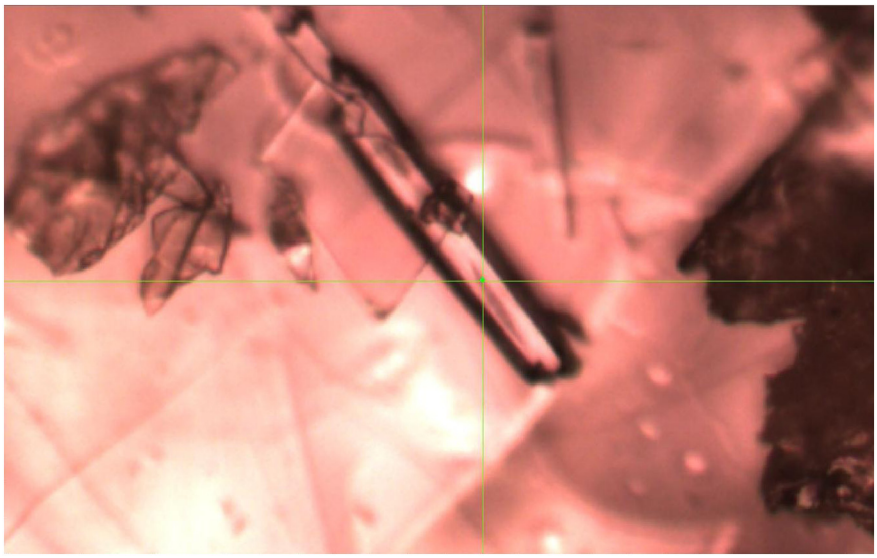

Fig. 10. The micro-photo of the crystalline sample that was extracted from the experimental cell after its slow cooling down with the subsequent slow depressurization and pumping out of the residual CO_2.

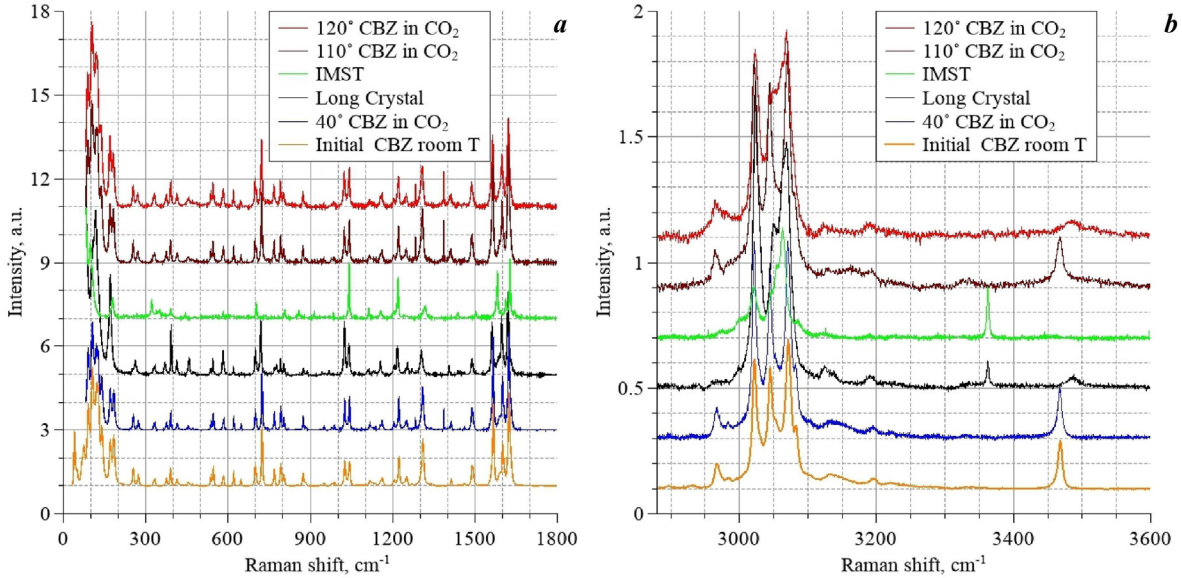

Fig. 11. The Raman spectra in two wavenumber ranges (0–1800 cm^{-1} and 2875–3600 cm^{-1}) of the crystalline sample extracted from the experimental cell (Long Crystal and IMST), as compared to that of pure CBZ polymorph III (initial CBZ form), as well as compared to the Raman spectra measured from the crystalline CBZ surface permanently contacting with CBZ saturated solution in $scCO_2$ at the temperatures of 40, 110, and 120°C (Ref. [18]) along the same isochore.

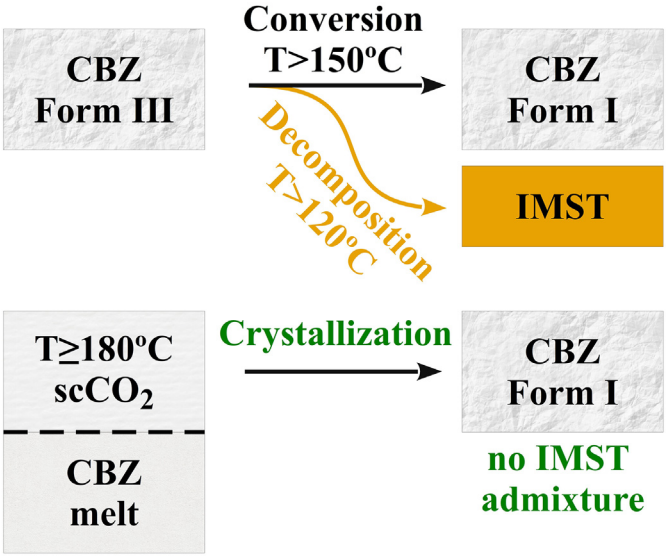

Fig. 12. Way to obtain the pure CBZ form III from CBZ saturated solution in $scCO_2$, being in contact with CBZ melt as compared to the high temperature conversion accompanied by CBZ decomposition.

ν(N—H) has a maximum at 3363 cm^{-1}), whereas the long needle crystals have spectral signatures of both IMST and CBZ polymorph I, whose characteristic spectral band of ν_s(H–N–H) has a maximum at 3487 cm^{-1} (see the spectrum «120°C CBZ in CO_2» measured at 120°C from the CBZ surface permanently contacting with CO_2 [18]). Moreover, the spectrum of the needle crystals does not show the spectral signatures of CBZ polymorph III, whose characteristic spectral band of ν_s (H–N–H) has a maximum at 3468 cm^{-1} (see the spectra: «Initial CBZ room T» and «40°C CBZ in CO_2» [18]). This fact means that the CBZ, which presents at 200°C preferably in tautomeric form, crystallizes into polymorph I when cooling down.

Thus, the obtained results showed that though the initial CBZ being in bottom phase of two-phase system partially decomposes with formation of IMST, the last has not been found in $scCO_2$ phase in the temperature range of (180–200°C). Such phenomenon is mainly related to the difference of CBZ and IMST solubilities in $scCO_2$ (solubility of IMST is much lower that is related to its molecular structure), as well as to the difference of their melting temperatures (T_{melt}(CBZ III) < 170°C, T_{melt} (IMST) = 197°C). Consequently, dissolution of CBZ in $scCO_2$ phase will lead to the IMST sedimentation from solution (salting out effect) without its melting. Therefore, one can suppose that if the RESS procedure is realized directly from the $scCO_2$ phase containing only the CBZ molecules existing in its tautomeric form, pure crystalline CBZ polymorph I (without an IMST admixture) can be obtained. Moreover, the probable admixture of ICA dissolved in $scCO_2$ will be also removed from the target product along with CO_2, upon their transition into the gaseous phase at adiabatic expansion.

5. Conclusions

In the present work, we perform a test of the high-temperature polymorphic conversion of CBZ in a $scCO_2$ medium. Here we studied the temperature range of 110–200°C along the isochore corresponding to the $scCO_2$ density equal to 1.3 of its critical value. In order to understand the conversion mechanism, here we also applied the IR technique developed by us and applied successfully in a number of our works. We performed a detailed analysis of the conformational equilibrium of the CBZ molecules in the $scCO_2$ phase, permanently contacting with an excess of CBZ, under isochoric heating conditions. We identified and studied three temperature ranges, where different types of CBZ–$scCO_2$ equilibria were realized. In the first one (110–140°C), it is the «CBZ solid – SCF solution» equilibrium. The second range (150–170°C) was characterized by a phase transition related to the CBZ melting in the high-density $scCO_2$ phase (at 160°C) that was accompanied by of opalescence in the SCF phase. In the third temperature range (180–200°C), the «CBZ melt – SCF solution» equilibrium took place.

Though, this study has a character of preliminary test, nevertheless even in this stage it allowed defining the phase diagram region where crystallization of CBZ from its solution in $scCO_2$ will give maximum yield of polymorph I. Thus, an analysis of the spectral data obtained for these three temperature ranges showed that only at the temperature above the phase transition region, when the «CBZ melt – SCF solution» equilibrium is realized, the $scCO_2$ phase contains one conformation of CBZ molecules. This finding allows us to suppose that it is possible to prepare pure crystalline CBZ polymorph I by crystallization from such $scCO_2$ phase. The advantages of such way can be schematically represented as follows (see Fig. 12). It was partially proved by the micro-Raman analysis of the crystalline substance extracted from the cell after the high-temperature experiment was finished.

The use of the high-temperature process for the production of pure CBZ polymorph I from a saturated SCF solution contacting with a melt phase has one more important advantage. It is the ability to significantly reduce the time required for reaching the CBZ equilibrium concentration in the $scCO_2$ phase. That is clearly proved by the IR spectroscopy results showing a considerable reduction in the time required for reaching the equilibrium concentration in comparison with the low-temperature process described in our previous work [18].

Author contribution

Roman D. Oparin: Conceptualization, Data curation, Formal analysis; Investigation; Methodology; Validation; Visualization; Writing - original draft.

Yevhenii A. Vaksler: Data curation, Formal analysis; Validation; Visualization; Editing.

Michael A. Krestyaninov: Formal analysis.

Abdenacer Idrissi: Writing - review & editing.

Michael G. Kiselev: Funding acquisition; Project administration; Resources; Supervision; Writing - review & editing.

Declaration of Competing Interest

The authors declare that they have no known competing financial interests or personal relationships that could have appeared to influence the work reported in this paper.

Acknowledgments

This work was financially supported by the Ministry of Science and Higher Education of the Russian Federation, grant No. RFMEFI61618X0097 and PHC Kolmogorov project, No. 41129RC.

The IR spectroscopy experiment was performed using the molecular fluid spectroscopy facility (http://www.ckp-rf.ru/usu/503933/) of G.A. Krestov Institute of Solution Chemistry of the Russian Academy of Sciences (ISC RAS) (Russia), the Raman experiment was performed in the Laboratory of IR and Raman Spectral Chemistry (LASIR) of the Lille University (France). The authors express their gratitude to M. Moreau (LASIR, Lille University) for her help with the Raman spectroscopy experiment.

References

[1] E. Thiruvengadam, G. Vellaisamy, Polymorphism in pharmaceutical ingredients a review, World J. Pharm. Pharm. Sci. 3 (2014) 621–633.

[2] J. Bernstein, P. Colman, J. Helliwell, K. Kantardjieff, T. Mak, P. Müller, Y. Ohashi, P. Paufler, H. Schenk, D. Viterbo, IUCr Monographs on Crystallography, 2002.

[3] S.R. Byrn, G. Zografi, S. Chen, Solid State Properties of Pharmaceutical Materials, Wiley Online Library, 2017.
[4] A.Y. Lee, D. Erdemir, A.S. Myerson, Crystal polymorphism in chemical process development, Ann. Rev. Chem. Biomol. Eng. 2 (2011) 259–280.
[5] H. Brittan, S. Vippagunta, D. Grant, Crystalline solids, Adv. Drug Deliv. Rev. 48 (2001) 3–26.
[6] J. Anwar, D. Zahn, Polymorphic phase transitions: macroscopic theory and molecular simulation, Adv. Drug Deliv. Rev. 117 (2017) 47–70.
[7] L. Padrela, M.A. Rodrigues, A. Duarte, A.M. Dias, M.E. Braga, H.C. de Sousa, Supercritical carbon dioxide-based technologies for the production of drug nanoparticles/nanocrystals–a comprehensive review, Adv. Drug Deliv. Rev. 131 (2018) 22–78.
[8] P. Girotra, S.K. Singh, K. Nagpal, Supercritical fluid technology: a promising approach in pharmaceutical research, Pharm. Dev. Technol. 18 (2013) 22–38.
[9] N. Esfandiari, Production of micro and nano particles of pharmaceutical by supercritical carbon dioxide, J. Supercrit. Fluids 100 (2015) 129–141.
[10] G.D. Hadiwinoto, P.C. Lip Kwok, R. Lakerveld, A review on recent technologies for the manufacture of pulmonary drugs, Ther. Deliv. 9 (2018) 47–70.
[11] A.Z. Hezave, F. Esmaeilzadeh, Micronization of drug particles via RESS process, J. Supercrit. Fluids 52 (2010) 84–98.
[12] A. Martín, M.J. Cocero, Micronization processes with supercritical fluids: fundamentals and mechanisms, Adv. Drug Deliv. Rev. 60 (2008) 339–350.
[13] Z. Knez, E. Weidner, Particles formation and particle design using supercritical fluids, Curr. Opinion Solid State Mater. Sci. 7 (2003) 353–361.
[14] Ž. Knez, M. Knez Hrnčič, M. Škerget, Particle formation and product formulation using supercritical fluids, Ann. Rev. Chem. Biomol. Eng. 6 (2015) 379–407.
[15] R.D. Oparin, M. Moreau, I. De Waele, M. Paolantoni, A. Idrissi, M.G. Kiselev, The interplay between the paracetamol polymorphism and its molecular structures dissolved in supercritical CO2 in contact with the solid phase: in situ vibration spectroscopy and molecular dynamics simulation analysis, Eur. J. Pharm. Sci. 77 (2015) 48–59.
[16] R.D. Oparin, D.V. Ivlev, A.M. Vorobei, A. Idrissi, M.G. Kiselev, Screening of conformational polymorphism of ibuprofen in supercritical CO2, J. Mol. Liq. 239 (2017) 49–60.
[17] R.D. Oparin, Y.A. Vaksler, M.A. Krestyaninov, A. Idrissi, S.V. Shishkina, M.G. Kiselev, Polymorphism and conformations of mefenamic acid in supercritical carbon dioxide, J. Supercrit. Fluids 152 (2019) 104547–104561.
[18] R.D. Oparin, M.V. Kurskaya, M.A. Krestyaninov, A. Idrissi, M.G. Kiselev, Correlation between the conformational crossover of carbamazepine and its polymorphic transition in supercritical CO2: on the way to polymorph control, Eur. J. Pharm. Sci. 146 (2020) 105273–105280.
[19] R.D. Oparin, D.V. Ivlev, M.G. Kiselev, Conformational equilibria of pharmaceuticals in supercritical CO2, IR spectroscopy and quantum chemical calculations, Spectrochim. Acta A Mol. Biomol. Spectrosc. 230 (2020) 118072–118080.
[20] I. Khodov, A. Dyshin, S. Efimov, D. Ivlev, M. Kiselev, High-pressure NMR spectroscopy in studies of the conformational composition of small molecules of ibuprofen in supercritical carbon dioxide, J. Mol. Liq. 309 (2020) 113113–113120.
[21] I.A. Khodov, K.V. Belov, S.V. Efimov, L.A.E.B.d. Carvalho, Determination of preferred conformations of mefenamic acid in DMSO by NMR spectroscopy and GIAO calculation, AIP Conf. Proc. 2063 (2019) 040007.
[22] I.A. Khodov, S.V. Efimov, V.V. Klochkov, G.A. Alper, L.A.E. de Batista Carvalho, Determination of preferred conformations of ibuprofen in chloroform by 2D NOE spectroscopy, Eur. J. Pharm. Sci. 65 (2014) 65–73.
[23] I.A. Khodov, S.V. Efimov, M.Y.U. Nikiforov, V.V. Klochkov, N. Georgi, Inversion of population distribution of Felodipine conformations at increased concentration in dimethyl Sulfoxide is a prerequisite to crystal nucleation, J. Pharm. Sci. 103 (2014) 392–394.
[24] M.M.J. Lowes, M.R. Caira, A.P. Lötter, J.G. Van Der Watt, Physicochemical properties and X-ray structural studies of the trigonal polymorph of carbamazepine, J. Pharm. Sci. 76 (1987) 744–752.
[25] I. Sovago, M.J. Gutmann, H.M. Senn, L.H. Thomas, C.C. Wilson, L.J. Farrugia, Electron density, disorder and polymorphism: high-resolution diffraction studies of the highly polymorphic neuralgic drug carbamazepine, Acta Crystallogr. Sect. B 72 (2016) 39–50.
[26] J.-B. Arlin, L.S. Price, S.L. Price, A.J. Florence, A strategy for producing predicted polymorphs: catemeric carbamazepine form V, Chem. Commun. 47 (2011) 7074–7076.
[27] P. Fernandes, K. Shankland, A.J. Florence, N. Shankland, A. Johnston, Solving molecular crystal structures from X-ray powder diffraction data: the challenges posed by γ-carbamazepine and chlorothiazide N,N,-dimethylformamide (1/2) solvate, J. Pharm. Sci. 96 (2007) 1192–1202.
[28] M. Lang, J.W. Kampf, A.J. Matzger, Form IV of carbamazepine, J. Pharm. Sci. 91 (2002) 1186–1190.
[29] C. Rustichelli, G. Gamberini, V. Ferioli, M.C. Gamberini, R. Ficarra, S. Tommasini, Solid-state study of polymorphic drugs: carbamazepine, J. Pharm. Biomed. Anal. 23 (2000) 41–54.
[30] A.L. Grzesiak, M. Lang, K. Kim, A.J. Matzger, Comparison of the four anhydrous polymorphs of carbamazepine and the crystal structure of form I, J. Pharm. Sci. 92 (2003) 2260–2271.
[31] I.A. Naguib, N.A. Elyazeed, F.A. Elroby, M.R. El-Ghobashy, Stability indicating spectrophotometric methods for quantitative determination of carbamazepine and its degradation product, iminostilbene, in pure form and pharmaceutical formulations, Spectrochim. Acta A Mol. Biomol. Spectrosc. 214 (2019) 21–31.
[32] L. Tian, S. Bayen, V. Yaylayan, Thermal degradation of five veterinary and human pharmaceuticals using pyrolysis-GC/MS, J. Anal. Appl. Pyrolysis 127 (2017) 120–125.
[33] T. Tandarić, V. Vrček, D. Šakić, A quantum chemical study of HOCl-induced transformations of carbamazepine, Org. Biomol. Chem. 14 (2016) 10866–10874.
[34] M.A.L. Pinto, B. Ambrozini, A.P.G. Ferreira, É.T.G. Cavalheiro, Thermoanalytical studies of carbamazepine: hydration/dehydration, thermal decomposition, and solid phase transitions, Braz. J. Pharm. Sci. 50 (2014) 877–884.
[35] Y. Takebayashi, K. Sue, T. Furuya, Y. Hakuta, S. Yoda, Near-infrared spectroscopic solubility measurement for thermodynamic analysis of melting point depressions of biphenyl and naphthalene under high-pressure CO2, J. Supercrit. Fluids 86 (2014) 91–99.
[36] H. Uchida, M. Yoshida, Y. Kojima, Y. Yamazoe, M. Matsuoka, Measurement and correlation of the solid−liquid−gas equilibria for the carbon dioxide + S-(+)-ibuprofen and carbon dioxide + RS-(±)-ibuprofen systems, J. Chem. Eng. Data 50 (2005) 11–15.
[37] R.M. Lemert, K.P. Johnston, Solid-liquid-gas equilibria in multicomponent supercritical fluid systems, Fluid Phase Equilib. 45 (1989) 265–286.
[38] N. Kalikin, M. Kurskaya, D. Ivlev, M. Krestyaninov, R. Oparin, A. Kolesnikov, Y. Budkov, A. Idrissi, M. Kiselev, Carbamazepine solubility in supercritical CO2: a comprehensive study, J. Mol. Liq. 311 (2020) 113104–113110.
[39] M.J. Frisch, G.W. Trucks, H.B. Schlegel, G.E. Scuseria, M.A. Robb, J.R. Cheeseman, G. Scalmani, V. Barone, B. Mennucci, G.A. Petersson, H. Nakatsuji, M. Caricato, X. Li, H.P. Hratchian, A.F. Izmaylov, J. Bloino, G. Zheng, J.L. Sonnenberg, M. Hada, M. Ehara, K. Toyota, R. Fukuda, J. Hasegawa, M. Ishida, T. Nakajima, Y. Honda, O. Kitao, H. Nakai, T. Vreven, J.A. Montgomery Jr., J.E. Peralta, F. Ogliaro, M. Bearpark, J.J. Heyd, E. Brothers, K.N. Kudin, V.N. Staroverov, T. Keith, R. Kobayashi, J. Normand, K. Raghavachari, A. Rendell, J.C. Burant, S.S. Iyengar, J. Tomasi, M. Cossi, N. Rega, J.M. Millam, M. Klene, J.E. Knox, J.B. Cross, V. Bakken, C. Adamo, J. Jaramillo, R. Gomperts, R.E. Stratmann, O. Yazyev, A.J. Austin, R. Cammi, C. Pomelli, J.W. Ochterski, R.L. Martin, K. Morokuma, V.G. Zakrzewski, G.A. Voth, P. Salvador, J.J. Dannenberg, S. Dapprich, A.D. Daniels, O. Farkas, J.B. Foresman, J.V. Ortiz, J. Cioslowski, D.J. Fox, Gaussian 09, Revision D.01, Gaussian, Inc., Wallingford CT, 2013.
[40] A. Austin, G.A. Petersson, M.J. Frisch, F.J. Dobek, G. Scalmani, K. Throssell, A density functional with spherical atom dispersion terms, J. Chem. Theory Comput. 8 (2012) 4989–5007.
[41] ChemSRC, Isocyanic Acid, [Online] https://www.chemsrc.com/en/cas/75-13-8_401667.html 2020.
[42] D. Belson, A. Strachan, Preparation and properties of isocyanic acid, Chem. Soc. Rev. 11 (1982) 41–56.
[43] M.E. Jacox, D.E. Milligan, Low-temperature infrared study of intermediates in the photolysis of HNCO and DNCO, J. Chem. Phys. 40 (1964) 2457–2460.
[44] N.H. Tho, Thermokinetic study of the isomerization of isocyanic acid, Vietnam J. Chem. 55 (2017) 478–483.
[45] NIST, Cyanic Acid, [Online] https://webbook.nist.gov/cgi/cbook.cgi?ID=C420053&Mask=800#ref-2 2020.